CFD MODELING OF FIRE SUPPRESSION AND ITS ROLE IN OPTIMIZING SUPPRESSANT DISTRIBUTION[*]

J. C. Hewson[†], S. R. Tieszen[‡], W. D. Sundberg[§]
Fire Science and Technology
Sandia National Laboratories
Albuquerque, NM 87185-1135

P. E. Desjardin[**]
Department of Mechanical and Aerospace Engineering
University at Buffalo
Buffalo, NY 14260-4400

Recent developments in suppression modeling for CFD codes are presented with an emphasis on fire suppression in cluttered environments. Suppression modeling is based on the ratio between the fluid mixing time scale and the flame chemical time scale. Flames are extinguished when the fluid mixing time is short relative to the chemical time required for combustion to occur. The effect of suppressants is to increase the required chemical time for combustion. Validation data sets are employed to evaluate the effectiveness of the suppression models in strained and obstructed flows. CFD results are used to indicate how changes in geometry may alter suppressant distribution. This approach supports design choices to provide optimal fire protection with minimal suppressant system weight and cost.

INTRODUCTION

Until their recent phase-out, chemicals like Halon 1301 (CF_3Br) and 1202 (CF_2Br_2) were widely employed to protect vehicles, structures and equipment from fire damage. Because of their high ozone-depleting potential, production of these fire-fighting agents has largely ceased, and research programs have identified a number of other promising agents [1]. Takahashi et al. [2] and Hamins et al. [3] have compiled data on the critical suppressant mole fraction required to suppress fires in various configurations for Halon 1301 and other potential fire suppressants. It is reported that non-ozone depleting agents identified with the most desirable toxicity, corrosion, stability, etc., characteristics generally require a greater agent mass and/or volume, relative to

[†] Corresponding and presenting author: jchewso@sandia.gov.
[‡] srtiesz@sandia.gov.
[§] wdsundb@sandia.gov.
[**] ped3@eng.buffalo.edu.

Halon 1301, to suppress a fire. For example, typical mole fractions of Halon 1301 required to suppress fires are between 3 and 4% while HFC-125 (C_2HF_5) requires between 8 and 9%. The mass of agent required is similarly greater, with roughly double the mass of HFC-125 required relative to that for Halon 1301. For applications where the fire suppression-system mass is a key design criterion, as it is in aircraft, a need to optimize the agent delivery system has been identified to minimize the additional suppression-system mass.

The optimization of fire-suppression systems in many applications is made more challenging by the fact that clutter in the form of structural supports, wiring, piping, machinery and similar items can adversely affect the suppressant flow. Furthermore, recirculation zones that form on the downstream sides of clutter have been identified as favorable for flame stabilization [4]. Of the various stabilized fires, liquid pool fires established behind obstructions such as structural ribs have been identified as some of the most challenging to suppress [4].

The present work addresses fire-suppression system optimization from a computational fluid dynamics (CFD) perspective, addressing specifically the problem of pool fires stabilized behind obstructions. A model suitable for predicting suppression within CFD codes is presented. This model has been implemented into the Vulcan fire-field model developed at Sandia National Laboratories in collaboration with and based on earlier work at the Norwegian Institute of Technology/ComputIt [5,6]. The suppression model is evaluated here using measurements of the agent required to suppress a fire stabilized behind a rearward-facing step [2]. The CFD code is then used to indicate ways in which the arrangement of clutter within an environment resembling an aircraft engine nacelle may change suppressant requirements, suggesting potential design practices that might be confirmed with further experimental measurements.

FIRE SUPPRESSION MODEL

The wide range of length scales in reacting flows presents a significant modeling challenge. Where flow rates are high enough that the flow is turbulent, as is typical in most terrestrial fire environments, fluid-mixing length scales may span several decades from the physical-system scale down to the Kolmogorov scales. Chemical length scales may be even smaller, typically less than a millimeter. Because it is not possible to computationally resolve the full range of scales, models of subgrid-scale processes are employed. Within the Vulcan fire-field model, the k-ε model [7] is employed to predict the effect of turbulent fluctuations on the flow while the eddy-dissipation concept (EDC) model [6] predicts the chemical evolution using a collection of perfectly stirred reactors (PSR).

PSR EQUATIONS

Combustion in Vulcan is modeled using the EDC model that can be thought of as a distribution of PSR's that relate the fuel-consumption rate to the fluid-mixing rate, the latter obtained from turbulent time scales. The submodels within Vulcan assume that the fuel-air mixing rates scale with the inverse of the Kolmogorov time scale, τ_K,

$$\tau_K = 0.41(\nu/\varepsilon)^{1/2} \tag{1}$$

where ν is the molecular viscosity and ε is the turbulent kinetic energy dissipation rate. The actual mass rate of reactant mixing is proportional to τ_K and also a function of the local reactant mass fractions. It is noteworthy that in high-fidelity modeling of turbulent diffusion flames, the fluid time scales corresponding to extinction are found to be very close to the Kolmogorov time scale [8]. Given this mixing rate, the species conservation equations for combustion within a PSR are

$$(Y_k^{prod} - Y_k^{reac}) / \tau_{PSR} = W_k \omega_k / \rho \tag{2}$$

where τ_{PSR} is the PSR mass divided by the rate of mass addition to the PSR, Y_k is the mass fraction of species k in the reactants or product streams, W_k is the molecular weight of k, ω_k is the molar production rate per unit volume and ρ is the product mixture density. The two mixing times scales, τ_K and τ_{PSR} are proportional and of the same magnitude but not exactly equal. The energy equation may be written similarly as

$$\sum_k (h_k^{prod} Y_k^{prod} - h_k^{reac} Y_k^{reac}) / \tau_{PSR} = \sum_k h_k^{prod} W_k \omega_k / \rho \tag{3}$$

where $h_k^1 = h_k^0 + \int_{T_0}^{T_1} c_{p,k} dT$ is the total enthalpy of species k at state 1, either the reactant or product state, where the temperature is T and c_p is the specific heat for species k. Conversion of reactants to products and the associated heat release occur either at a rate determined by either the mixing rate, $1/\tau_{PSR}$, or at a maximum chemical rate that is a function of the reactant composition. Fires are typically mixing limited, but if τ_{PSR} is sufficiently small (fast mixing) then conversion of reactants to products and the associated heat release cannot proceed to completion. This results in a reduction in temperature leading to a reduction in chemical rates, the chemical reaction rates being greatly reduced at lower temperatures. Continued reduction in the mixing time relative to the chemical time leads eventually to a state where no combustion is possible and the flame is extinguished. The ratio between fluid and chemical mixing times is generally referred to as the Damköhler number, $Da = \tau_K / \tau_{chem}$. A suitable chemical time relevant to flame extinction, τ_{ext}, can be defined as the value of τ_{PSR} corresponding to a switch from combustion occurring to combustion being impossible. τ_{ext} is the chemical time scale representing the fastest possible chemical reaction rates. For Damköhler numbers smaller than a critical value, Da_{crit}, the flame will be extinguished, so that for

$$\tau_K / \tau_{ext} > Da_{crit} \tag{4}$$

combustion may occur, while for

$$\tau_K / \tau_{ext} < Da_{crit} \tag{5}$$

combustion may not occur. The critical Damköhler number that relates τ_K and τ_{ext} is not known a priori and is determined empirically by matching blow-off criteria for an ethane jet flame as described in [9]; a value of $Da_{crit} = 0.563$ is obtained in this manner. The suppression model used in the present work takes advantage of this Damköhler number criteria by determining values of τ_{PSR} corresponding to extinction, giving τ_{ext}, from detailed chemical-kinetic calculations in the PSR configuration.

The chemical time scale is a function of the reactant mass or mole fractions, enthalpy and the pressure. For the present purposes, the discussion will focus on the effect of reactant mass or mole fractions, assuming these reactants originate at ambient pressures and temperatures, and neglecting enthalpy changes. While it is straightforward to make the chemical time scale a function of the enthalpy, and this has been done with the suppression model, the added parameter space complicates the current discussion. Furthermore, the results then depend strongly on heat flux through walls, a quantity that is not well known for the experimental configurations under consideration here. (Two neglected thermal effects that are of moderate significance: For JP-8 pool fires considered here, the initial fuel vapor temperature is somewhat greater than ambient; this tends to reduce the chemical time scale. Radiative thermal losses and losses to the walls, while included in Vulcan, are currently neglected in the suppression model because the magnitude of these losses are dependent on the wall heat flux which is not known. Estimates indicate that heat losses to obstructions are significant here and tend to increase the chemical time scale.)

Within Vulcan, chemical reactions are greatly simplified, reflecting the predominance of mixing processes in fires. This simplified treatment of kinetics is not necessarily sufficient for suppression predictions, and chemical time scales corresponding to suppressant addition are calculated off-line. These off-line calculations use the Chemkin PSR capability [10] with a detailed chemical mechanisms for iso-octane from Curran et al. [11] coupled with a mechanism for halogenated suppressants from Babushok et al. [12]. Chemical time scales have been obtained for iso-octane combustion in air with HFC-125, N_2, H_2O, CO_2 and CF_3Br although only results with the first suppressant are described here. Chemical time scales relevant to suppression are obtained by conducting PSR simulations at successively shorter residence times, τ_{PSR}, until combustion is extinguished, defining τ_{ext}. To facilitate use in CFD simulations, values for τ_{ext} are fit to a suitable functional form as a function of the mole fraction of HFC-125 added to the inlet air, $X_{HFC-125,ext}$. For iso-octane, the selected surrogate for JP-8, the curve fit, inverted to express the magnitude of $X_{HFC-125,ext}$ required to extinguish the mixture given τ_K, is

$$X_{HFC-125,ext} = X_1 \frac{(1+A)\sigma^B}{(A+\sigma^B)} \tag{6}$$

where $\sigma = (\tau_{ext} - \tau_0)/(\tau_1 - \tau_0)$ is the normalized mixing time, τ_0 is the value of τ_{ext} when no suppressant is present, $\tau_1 = 0.01$ s is an arbitrary long residence time at which $X_1 = 0.1255$ is the quantity of HFC-125 required to induce extinction, and $A = 0.1596$ and $B=0.6523$ are constants for a fixed enthalpy and fuel type. In general the quantities A, B and X_1 have been

determined and curve fit as a function of enthalpy, fuel and suppressant type, but only the indicated values are required for the present results.

Given the chemical time scale as a function of the fluid cell composition and the mixing rate based on the dissipation rate and viscosity (through the Kolmogorov time scale), the magnitude of the Damköhler number in that cell determines whether combustion takes place in that cell or not based on Eqs. 4 and 5. In the numerical implementation, given τ_K in a fluid cell from Eq. 1, τ_{ext} is obtained from Eqs. 4 and 5, from which $X_{HFC-125}$ required to extinguish the flame is obtained using Eq. 6; comparison with the fluid cell HFC-125 mole fraction indicates whether suppression occurs. A similar approach was used by Byggstoyl and Magnussen for local quenching in the absence of suppressants [13].

THE FLUID DYNAMICS OF SUPPRESSION

As noted in the Introduction, flow obstructions can act as flame holders, stabilizing flames and making suppression difficult. Stabilization is aided by creating a recirculation region with relatively low dissipation rates, and thus large τ_K, and hot products. Suppression is made more difficult because it takes significantly more time for suppressant to penetrate the recirculation zone than it takes for the suppressant to pass over an unobstructed flame. Hamins et al. and others [2,3,14] have taken advantage of a simple mixing model in the form of the conservation equations for an unsteady PSR [10] that predicts the suppression delay associated with the delay in mixing suppressant into a recirculation zone. The model predicts that the mole fraction of suppressant in the recirculation zone varies as

$$X_{recirc} = X_{\infty}[1 - \exp(-t/\tau_{mix})] \tag{7}$$

where X_{∞} is the suppressant mole fraction outside the recirculation region and $\tau_{mix} \propto h/u^*$ is the mixing time, proportional to the quotient of the velocity past the recirculation zone and the recirculation zone thickness, here taken to be the step height, h. Takahashi et al. measured the proportionality constant for their configuration (Case A1 here) to be $\tau_{mix} = 34.7(h/u^*)$ where u^* is explicitly given as the average of the mean flow velocity over the step and the mean flow without the step [15].

MODEL EVALUATION

For a CFD model to adequately predict suppression in the presence of obstructions, it will be important that the model can reasonably predict (1) the suppressant required to extinguish flames at a given fluid mixing rate, and (2) the rate of suppressant mixing into recirculation regions. To address these questions, simulations using the suppression model described above were conducted for JP-8 pool fires stabilized behind a backwards-facing step, and results are compared with measurements of Takahashi et al. [2]. Those simulations for which there are experimental data available and that are involved in model evaluation are referred to as Case A1; see Table I. All simulations denoted as Case A are conducted in a 154 mm by 154 mm square wind tunnel, 770 mm long, with a 64 mm tall backwards-facing step placed in front of a 150 mm by 150 mm JP-8 pool. Air flow through the wind tunnel was 10100 slpm, the turbulence level at

the entrance was set to 6% and the turbulent length scale, used to calculate the initial dissipation rate was set to 3 mm based on the turbulence generators employed in the experiments. Figure 2 provides an overview of the simulation geometry, showing the location of the flame behind the step. Simulations were brought to a steady state with fires established, after which suppressant

Table I: Summary description of simulations

Case	Description	τ_{mix}
A1[*]	As in Takahashi et al. [2] with the fuel being JP-8 and the suppressant being HFC-125.	0.23 s
A3	As in A1 but with a 42 mm rib on the upper wall collocated with the backwards-facing step.	0.15 s
A5	As in A1 but with a 42 mm rib on the upper wall 84 mm behind the backwards-facing step.	0.24 s
B1	22.5 cm high, 180 cm wide and 180 cm long wind tunnel with 5 cm rib locate 60 cm from entrance. A 45 cm long by 30 cm wide JP-8 pool is centered on the lower surface.	0.30 s
B2	As in B1 but with two 5 cm high longitudinal ribs each located 20 cm from the centerline.	0.30 s
C1	As in B1 but with the tunnel height reduced to 10 cm.	0.23 s
C2	As in B2 but with the tunnel height reduced to 10 cm.	0.23 s

[*] Used in model validation.

was injected, thoroughly mixed with the incoming air. Figure 3 shows the state along the wind tunnel centerline just prior to agent injection with the high temperature flame mainly located at the edge of the recirculation zone between the fuel and air. Fuel vaporization is determined by the rate of heat flux to the pool surface, moderated by an estimate of heat losses, for example to the porous plate through which the fuel passes. The flame location relative to the edge of the recirculation zone is somewhat sensitive to these heat losses. It was assumed that 40% of the heat flux to the pool resulted in fuel vaporization. Greater heat losses result in reduced fuel vaporization, bringing the flame closer to the pool. This effect tends to increase the heat flux to the pool, partially offsetting the heat losses. The sensitivity to heat loss is not very large, but it is enough to move the flame in and out of the recirculation zone given 80% to zero heat losses. Also shown in Fig. 3 is a cross-section of the computational mesh, showing grid points clustered around the step to capture relevant details of the boundary layer in these regions. Grid sensitivity studies are in process, although refinement in regions around the step to date has not resulted in measurable differences in the results for Case A1. Injection of suppressant is conducted by keeping the air mass flow rate through the domain constant and increasing the total mass flow rate as required to inject the desired quantity of suppressant.
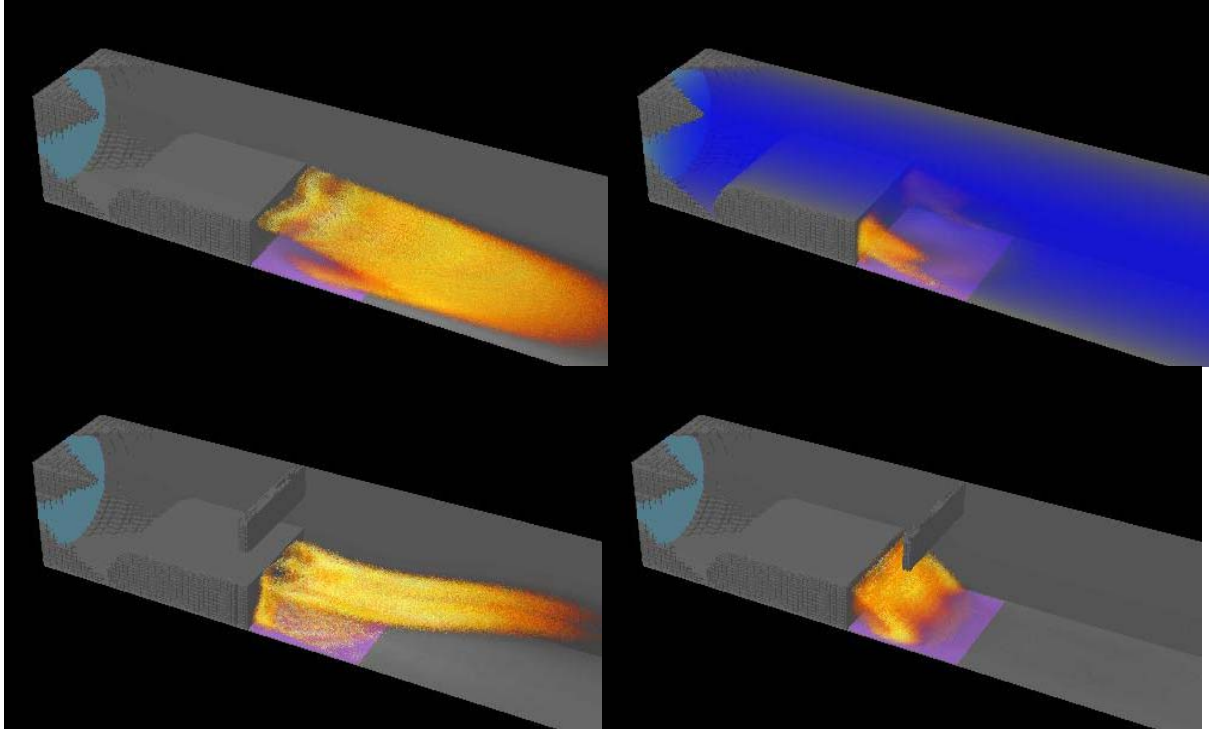
Figure 2: Ray tracing image of Case A1 before agent injection (top left) and 0.2 s after injection of 10% HFC-125 (top right). Images of Case A3 (lower left) and A5 (lower right) before agent injection. The air/suppressant inlet is light blue, the pool is purple, the suppressant is deep blue and the flame is orange to yellow.

Rather than conduct a number of simulations for each suppressant mole fraction to determine the minimum injection time, as were done in the experiments, the suppressant was continually injected and the time to suppression was measured. Suppression was defined as the time at which the maximum temperature throughout the domain dropped below 1000 K. Figure 4 (a) shows the evolution of the maximum temperature for various suppressant mole fractions. The selection of 1000 K as the temperature corresponding to suppression seems justified here since the temperature rapidly drops around this point and there is no evidence of tendency to reignite for temperatures below 1200 K. It is evident that an HFC-125 mole fraction of 0.075 is insufficient to suppress this flame while 0.08 is sufficient. Successively greater mole fractions lead to a monotonic reduction in the time required to suppress the flame. These results are summarized in Fig. 4 (b) where they are also compared with the results of Takahashi et al. [2].
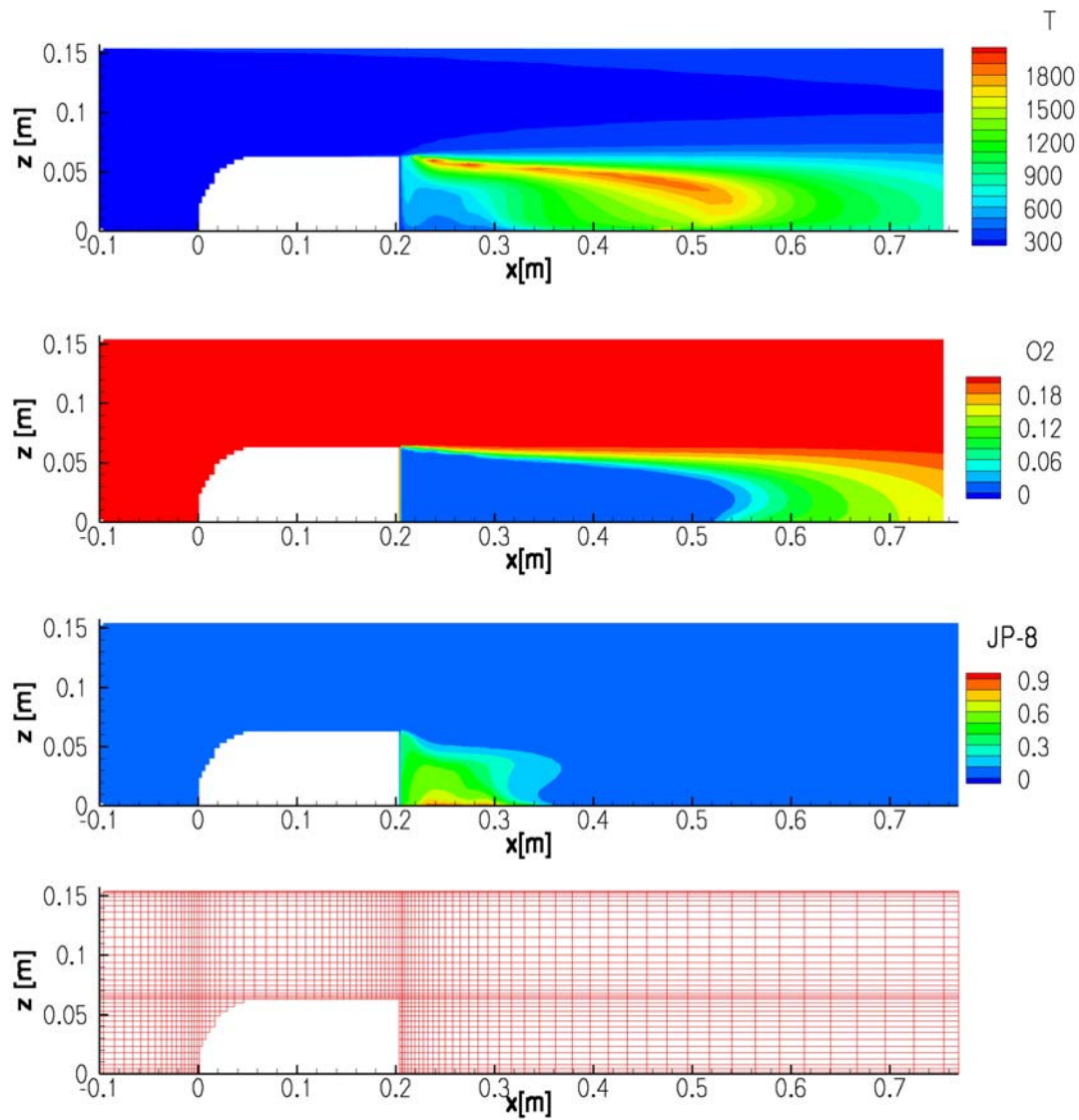
Figure 3. Centerline contour plots showing (from top to bottom) the temperature, oxygen mass fraction, fuel mass fraction and the computational grid for Case A1
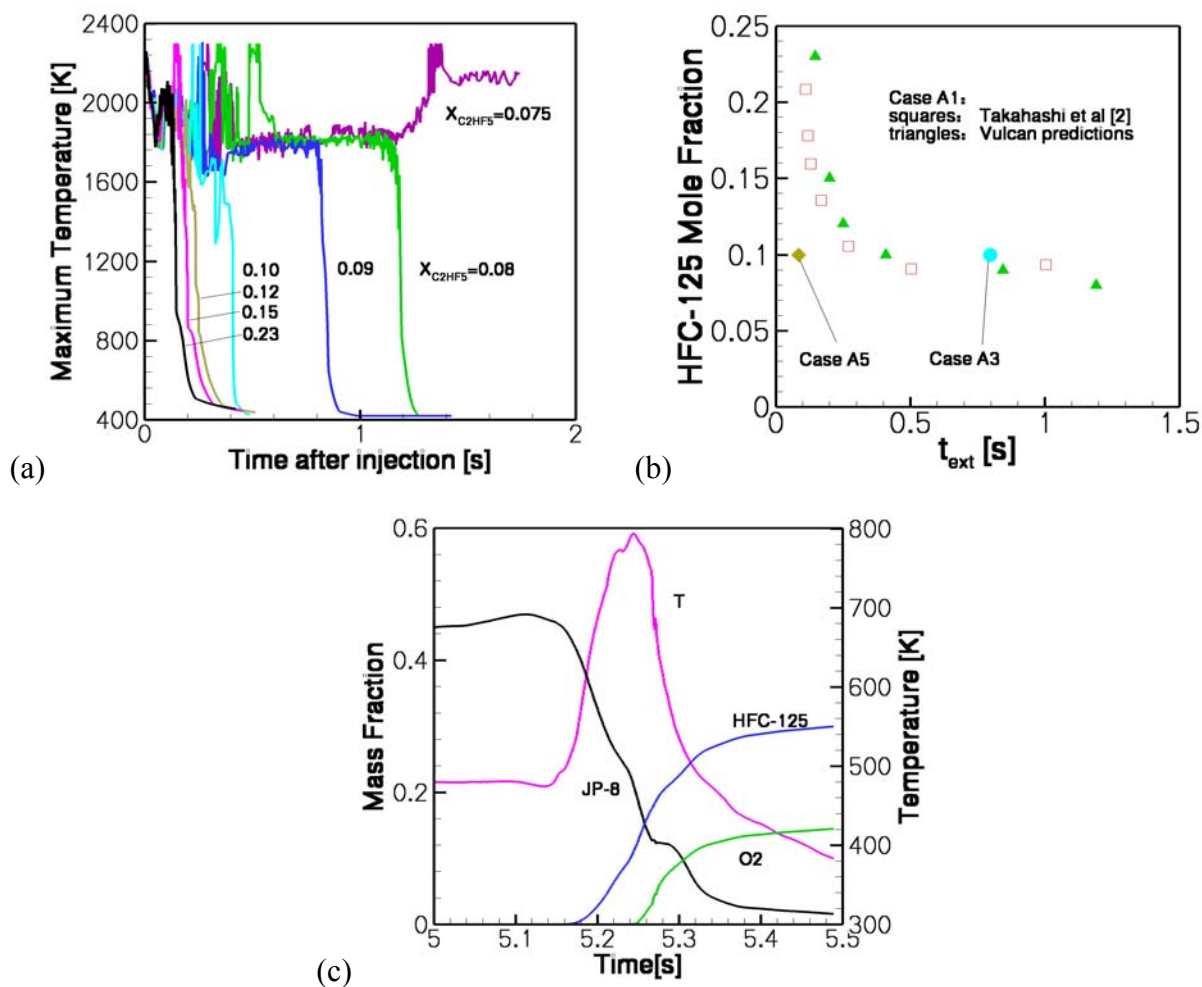
(a)

(b)

(c)

Fig 4. (a) Evolution of the maximum fluid cell temperature in the domain for Case A1 for various HFC-125 mole fractions. (b) Suppression times as a function of HFC-125 mole fraction for Cases A1, A3 and A5. (c) Mass fraction and temperature evolution in the recirculation zone (8mm above pool and 8mm behind step) for Case A1 with 10% mole fraction HFC-125 injected at 5 seconds.
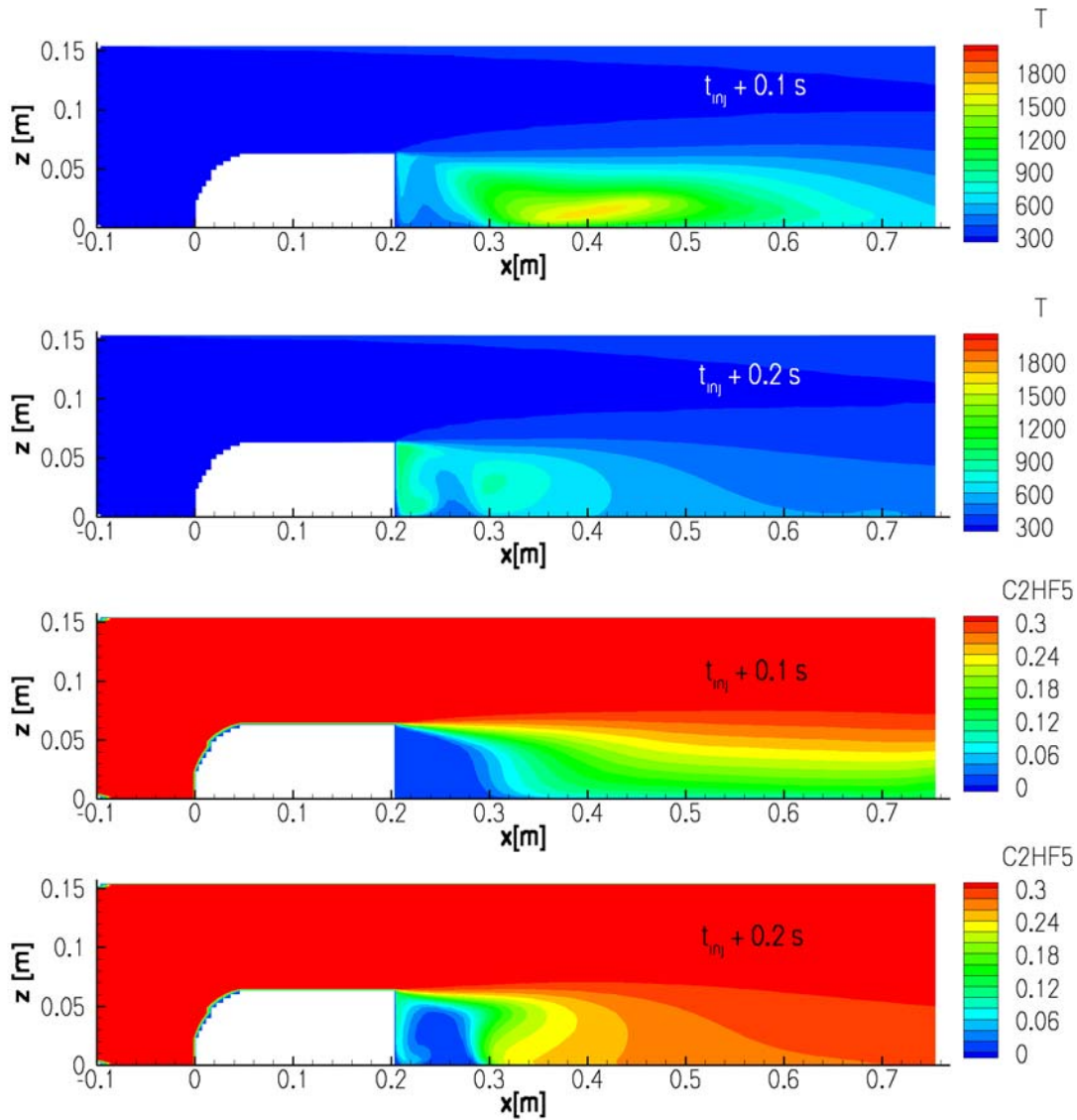
Figure 5. Centerline contour plots showing the temperature and HFC-125 mass fraction at 0.1 and 0.2 s after suppressant injection for Case A1 with 0.1 HFC-125 mole fraction injected

The maximum temperature shown in Fig. 4 (a) fluctuates greatly during the transient suppression process because of a combination of the refined grid and the delta-function nature of the EDC model: at certain instants of time the model treats a particular cell as almost entirely stoichiometric flame. This behavior occurs as the flame moves through the finely gridded region behind the step during the suppressant injection. While this behavior would not be observed when averaging over integral time or length scales, this can occur in the context of the EDC model when the cell thickness is comparable to the Kolmogorov scale as it is in the present grid at some locations. In fact, for better EDC model applicability, it is desirable to coarsen the mesh, but high levels of grid refinement are used to reduce reliance on log-linear wall models in regions of adverse pressure gradients.

10

Figure 4(c) shows the local smoothness of the temperature evolution deep in the recirculation region along with major species. This figure and Fig. 5 show key aspects of the suppression dynamics for the particular case A1 with 0.1 HFC-125 mole fraction.   The suppressant rapidly flows over the top of the recirculation zone, but dilatation associated with combustion initially reduces recirculation behind the step. As the upper portions of the flame are suppressed (within the first 0.1 s) recirculation gradually increases, bringing suppressant in to extinguish regions that are still burning. As the fire suppression progresses, the flame is observed in Figs. 4(c) and 5 to move deeper into the recirculation zone as fuel vaporization is reduced and oxygen moves into the recirculation zone with the suppressant. It is found that an inner, secondary recirculation zone forms in the corner between the pool and the step into which some air is entrained, primarily from the sides, but into which suppressant penetration is exceedingly slow. With wall heat losses treated in the suppression model, this region is generally the last to be suppressed.

CFD FOR OPTIMIZING FIRE SUPPRESSION

The above results indicate the potential to predict fire suppression behavior. In the following sections, we describe how Vulcan is applied to answer questions of interest both in the aircraft design and in the design of experimental facilities to address key questions related to fire-suppression physics.

RELATIVE LOCATIONS OF CLUTTER

Using the same basic configuration as the experiments conducted by Takahashi et al., simulations were conducted to investigate the effect of additional clutter, in the form of a small rib on the upper wall, opposite the backwards-facing step behind which the fire is stabilized. Specifically, a rib protruding from the upper surface with a height of 42 mm is located either directly above the end of the backward facing step or two rib heights behind the back of the step; these configurations are denoted A3 and A5; the simulations are otherwise similar to those in A1. These scenarios reflect the existence of additional clutter on the side of a passage opposite the flame-stabilizing obstruction. Additional obstructions result in the acceleration of the flow over the step and past the fire. The correlation between flow velocities over obstructions and suppressant mixing rates [2,3,14,15] would suggest that collocated obstructions would result in accelerated suppression. In Fig 4(c), suppression times are plotted for cases A3 and A5 with 10% HFC-125 suppressant in the free stream along with the results for Case A1 where there is no additional obstruction. The results are not completely intuitive: there is a strong reduction in suppression time for case A5 but no reduction and possibly an increase in suppression time for case A3. This trend goes against a simple implementation of Eq. 7 that would suggest reduced suppression times in accordance with the changes of τ_{mix} in Table I. Equation 7 would imply that case A3 should have the shortest suppression time while it is observed to have the longest.

The results for cases A3 and A5, relative to A1, can be explained by consideration of the pressure field, shown in Fig. 6, that determines the extent of the recirculation regions. Also shown in Fig. 6 are velocity vectors and streamline traces from behind the corner of the step to provide rough indications of recirculation zone sizes.   In case A3, flow past a flat plate oriented against the flow results in a greater pressure loss than flow over the backwards-facing step. The greater pressure loss tends to pull the mean flow upward, reducing the mixing in the lower
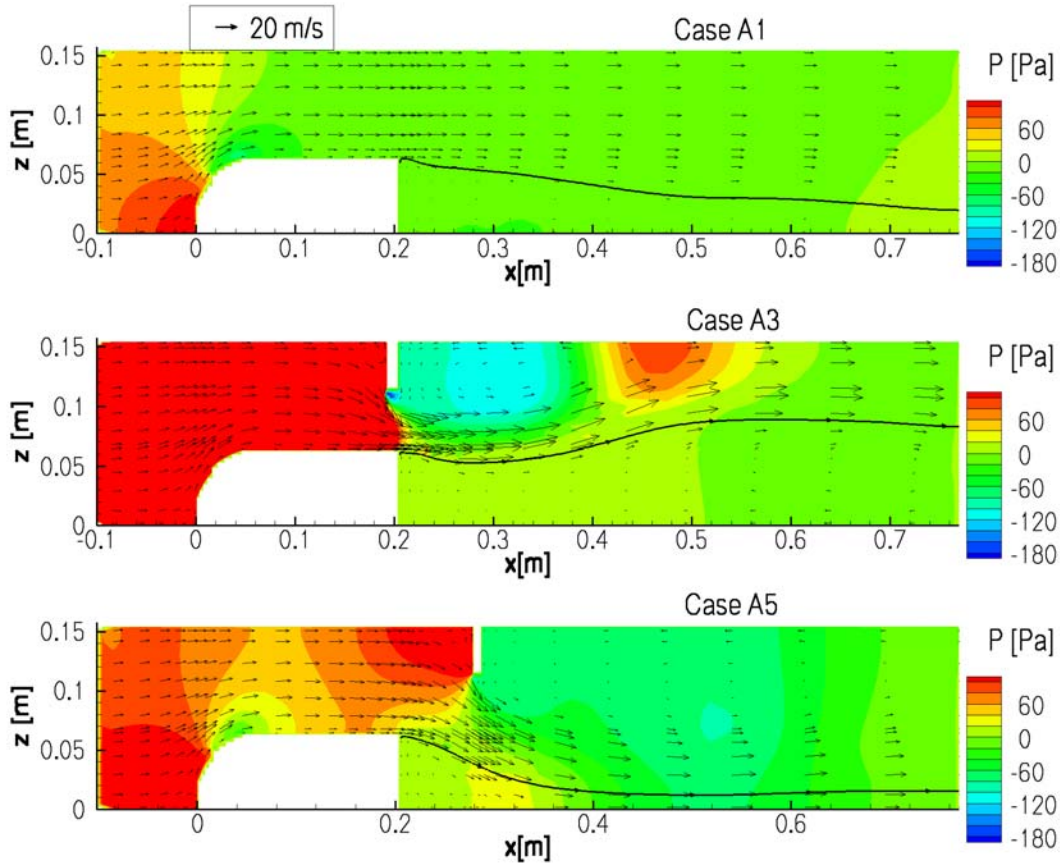
Figure 6: Centerline pressure contours and velocity vectors for Cases A1, A3 and A5 prior to suppressant injection. Contour levels are equal for all panes and space at 20 bar intervals. Solid lines represent streamline traces from just behind the corner of the step.

recirculation zone where the fire is stabilized. Shifting the upper obstruction past the step results in significant reductions in the suppression time. This result occurs because the high-pressure region in front of the upper rib is coincident with the low-pressure region behind the backwards-facing step, accelerating the flow downward and increasing suppressant mixing into the recirculation zone. Thus, despite the fact that the area available for flow past the lower recirculation zone is greater and the velocity u^* correspondingly lower in Case A5 relative to Case A3, the suppression time is reduced because the flow is directed into the recirculation zone, thereby increasing mixing in the recirculation zone. The key result is that the suppression time is strongly dependent on recirculation zone size, and that multiple factors affect the recirculation zone size. Given a single obstruction, recirculation zone mixing is primarily dependent on h/u^*, but pressure gradients can change the effective recirculation zone thickness. Given this, recirculation region mixing times should be a function of h^*/u^*, where $h^* = h^*(h, \nabla p)$, indicating the dependence of the effective recirculation zone length scale on the pressure gradient. As is typical for separated flows, favorable (accelerating) pressure gradients reduce recirculation zone length scales while adverse pressure gradients have the opposite effect. Pressure drop past obstructions is related to the drag coefficient, and there is extensive literature on the subject that may be useful in identifying the magnitude of pressure changes across obstructions. We note here that the k-ε model is known to have limited success in adverse pressure-gradients, but the

conclusions reached here are not dependent on the validity of the k- ε model. Rather, the conclusions depend on the relevance of pressure gradients in directing fluid flow, and on the result from dimensional analysis that mixing times can be related to u^* and the characteristic scale of the recirculation zone.

ASPECT RATIO EFFECTS

The model validation experiments described above and others for studying fire suppression of obstruction-stabilized flames [2,3] were conducted in roughly square wind tunnels. In certain applications such as aircraft engine nacelles, the width to height aspect ratio tends to be large. In preparation for studies of actual engine nacelle environments and to plan an additional series of experiments to be conducted at WPAFB by the USAF 46 Test Wing [16] a series of simulations using dimensions characteristic of the wind tunnel available at WPAFB and an F-18 engine nacelle were conducted. The characteristic dimensions identified are obstruction heights on the order of 5 cm in wide channels with heights on the order of 10 to 30 cm. The resulting series of simulations, cases B1, B2, C1 and C2 are summarized in Table I. In each of these simulations, the inlet velocity was 5 m/s, the turbulence intensity was 10% and the turbulent length scale was 0.025 m. Significantly, pool sizes are narrow relative to the channel width. Simulations indicate that dilatation from a pool fire behind a rib induces secondary recirculation regions that sweep the fire outward and along the rib transverse to the flow.   Observation of these flow fields indicates that they may reduce the suppressant penetration into certain portions of the flame-stabilization region. However, within aircraft, structural supports and clutter are observed to be oriented in both transverse and longitudinal directions. The consequences of longitudinal (streamwise) ribs are examined by adding longitudinal ribs just outside of the pool (Cases B1 and C1 becoming Cases B2 and C2). It is observed that for both Cases B2 and C2 the longitudinal ribs do not prevent spread of the fire beyond the ribs, as shown in Fig. 7. Mass fraction profiles in the recirculation zone indicate, however, that longitudinal ribs do affect the flow because rate of transport of agent is greater with ribs for Case B2 relative to B1 and for Case C2 relative to C1, shown in Fig. 8(a). Further, the time to suppress the fire is reduced as shown in Fig. 8(b). The result that longitudinal ribs reduce the time required to suppress a fire suggest a series of experiments in high aspect ratio wind tunnels to evaluate their validity. If the experiments are consistent with the simulation results, then both the potential reduced suppression ability due to dilatation and the possibility that longitudinal clutter ameliorates it are considerations in system design.

SUMMARY

A suppression model based on a critical Damköhler number for extinction and suitable for use in CFD codes has been presented. Chemical time scales for suppression are obtained using PSR calculations with detailed chemistry to determine the PSR mixing time that corresponds to extinction. As suppressants are mixed with reactants, chemical time scales increase leading to easier suppression. These time scales are related through the Damköhler number to fluid times scales based on the Kolmogorov time scale.
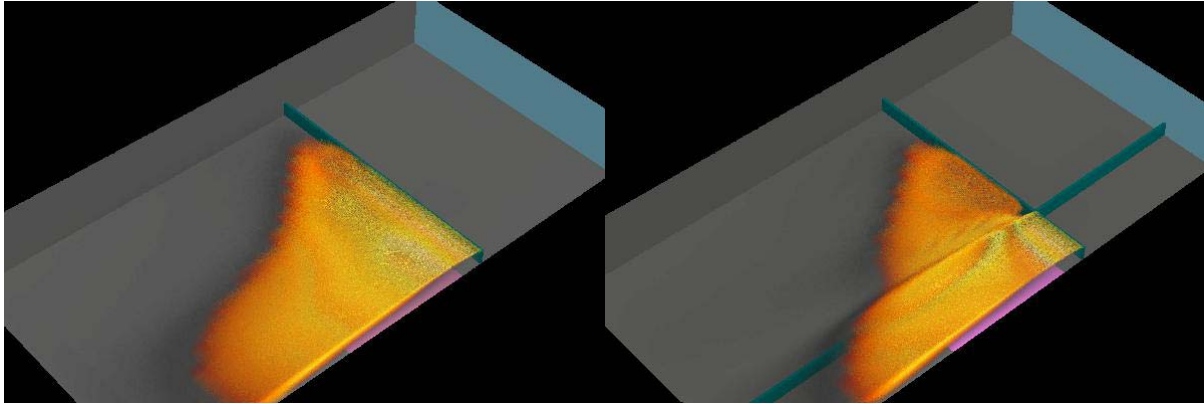
Figure 7: Raytracing images of cases B1 (left) and B2 (right). Colors as in Fig. 2. Simulations take advantage of symmetry and only the calculated half of the domain is shown.
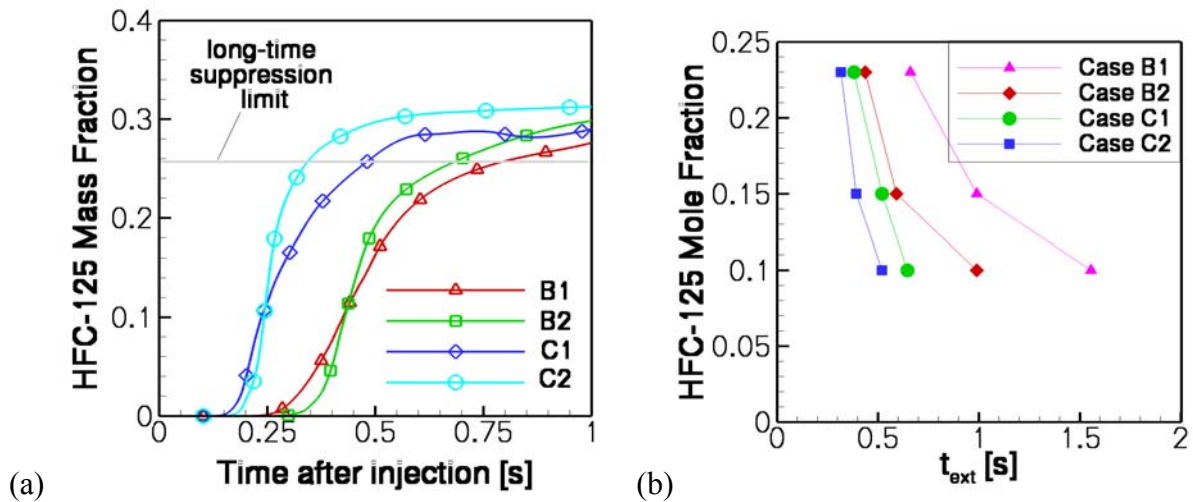

(a)   (b)

Figure 8: (a) Temporal evolution of HFC-125 mass fraction in the recirculation zone at a point 0.012 m above the lower surface and 0.05 m behind the rib along the centerline. (b) Suppression times as a function of HFC-125 mole fraction for Cases B1, B2, C1 and C2.

This model has been implemented into the Vulcan fire field model and evaluated through comparison with measurements of suppression of a pool fire in a wind tunnel behind a step. Suppression of obstruction-stabilized fires is dependent on mixing of the suppressant into recirculation regions. To leading order, this mixing time is proportional to the velocity past an obstruction and the characteristic length scale for the recirculation region. Simulations were also conducted for perturbations on this flow in the form of additional clutter, a large width-to-height aspect ratio, and longitudinal ribs. Results indicate that these result in flow variations leading to differing suppressant mixing times. Pressure changes across obstructions, flow dilatation due to combustion and streamwise obstructions have all been identified as influencing suppressant mixing times.

14

REFERENCES

[1] A. Hamins, G. W. Gmurczyk, W. L. Grosshandler, R. G. Rehwoldt, I. Vazquez, T. Cleary, C. Presser, K. Seshadri, "Flame Suppression Effectiveness," in *Evaluation of Alternative In-Flight Fire Suppressants for Full-Scale Testing in Simulated Aircraft Engine Nacelles and Dry Bays. Section 4*, W. L. Grosshandler, R. G. Gann, W. M. Pitts, Editors, pp. 345-465 (1994).

[2] F. Takahashi, W. J. Schmoll, E. A. Strader, V. M. Belovich, "Suppression Behavior of Obstruction-Stabilized Pool Flames," *Combust. Sci. Tech.*, 163:107-130 (2001).

[3] A. Hamins, T. G. Cleary, P. Borthwick, N. N. Gorchkov, K. B. McGrattan, G. P. Forney, W. L. Grosshandler, C. Presser, L. Melton, "Suppression of Engine Nacelle Fires," in *Fire Suppression System Performance of Alternative Agents in Aircraft Engine and Dry Bay Laboratory Simulations. Volume 2*, Gann, R. G., Editor, pp. 1-199 (1995).

[4] R. Hirst, D. Sutton, *Combust. Flame*, 5:319 (1961). R. Hirst, P. J. Farenden, R. F. Simmons, *Fire Technol.*, 12:266 (1976). R. Hirst, P. J. Farenden, R. F. Simmons, *Fire Technol.*, 13:59 (1977).

[5] J. Holen, M Bronstrom, B. F. Magnussen, "Finite Difference Calculation of Pool Fires," *Proc. Combust. Instit.*, 27:1677-1683 (1990).

[6] B. F. Magnussen, "The Eddy Dissipation Concept," *Proceedings of the Eleventh Task Leaders Meeting*, IEA Working Group on Conservation in Combustion, Lund, Sweden (1989).

[7] W. P. Jones, B. E. Launder, "Prediction of Laminarization with a 2-Equation Model of Turbulence," *Int. J. Heat Mass Transfer*, 15:301 (1972).

[8] J. C. Hewson, A. R. Kerstein, "Local Extinction and Reignition in Nonpremixed Turbulent CO/H2/N2 Jet Flames," *Combust. Sci. Tech*, 174:35-66 (2002).

[9] S. R. Tieszen, D. W. Stamps, T. J. O'Hern, " A Heuristic Model of Turbulent Mixing Applied to Blowout of Turbulent Jet Diffusion Flames," *Combust. Flame*, 106:442-466 (1996).

[10] E. Meeks, H. K. Moffat, J. F. Grcar, R. J. Kee, "AURORA: A Fortran Program for Modeling Well Stirred Plasma and Thermal Reactors with Gas and Surface Reactions," Sandia National Laboratories Report SAND96-8218 (1996).

[11] H. J. Curran, P. Gaffuri, W. J. Pitz, C. K. Westbrook, "A Detailed Modeling Study of Iso-Octane Oxidation," *Proc. Combust. Instit.*, 27:381-395 (1999).

[12] V. I. Babushok, T. Noto, D. R. F. Burgess, A. Hamins, W. Tsang, "Influence of CF3I, CF3Br, and CF3H on the High-Temperature Combustion of Methane," *Combust. and Flame*, 107:351-367 (1996).

[13] S. Byggstoyl, B. F. Magnussen, "A Model for Flame Extinction in Turbulent Flow," *Proc. Combust. Instit.*, 17:381-395 (1978).

[14] Hamins, A.; Presser, C.; Melton, L., "Suppression of a Baffle-Stabilized Spray Flame by Halogenated Agents." *Proc. Combust. Instit.*, 26:1413-1420 (1996).

[15] F. Takahashi, W. J. Schmoll, E. A. Strader, V. M. Belovich, "Suppression of a Nonpremixed Flame Stabilized by a Backward-Facing Step," *Combust. Flame*, 122:105-116 (2001).

[16] P. J. Disimile, J. R. Tucker, private communication (2002).